JCTC Journal of Chemical Theory and Computation

Article

pubs.acs.org/JCTC

Current vs Charge Density Contributions to Nonlinear X-ray Spectroscopy

Jérémy R. Rouxel,* Markus Kowalewski,* and Shaul Mukamel*

Department of Chemistry, University of California, Irvine, California 92697-2025, United States

ABSTRACT: Stimulated (coherent) and spontaneous (incoherent) nonlinear X-ray signals are expressed using a spatially nonlocal response tensor which directly connects them to the time evolving current **j** and charge σ densities rather than to electric and magnetic multipoles. The relative contributions of the $\sigma\mathbf{A}^2$ and $\mathbf{j}\cdot\mathbf{A}$ minimal coupling terms, where **A** is the vector potential, are demonstrated. The two dominate off-resonant and resonant scattering, respectively, and make comparable contributions at near resonant detunings.

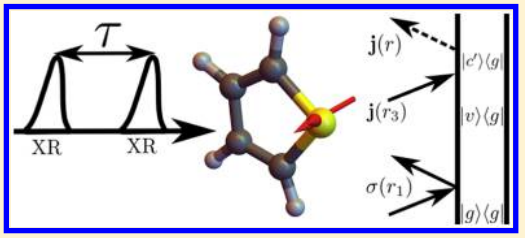

1. INTRODUCTION

Recent development of bright ultrafast coherent X-ray sources, such as free electron lasers (XFEL)[1] or high harmonic generation (HHG),[2] has triggered intense research activity aimed at the experimental realization of all-X-ray nonlinear spectroscopy.[3−5] Combined with other advances in single molecule spectroscopy[6] and ultrafocusing of beams,[7,8] this opens up new opportunities to create real time movies of chemical reactions.

This article applies a nonlocal response formalism based on the minimal coupling Hamiltonian of light-matter interaction to the X-ray regime. Extending the standard response function theories[9−11] using the minimal coupling Hamiltonian permits one to include the spatial variation of the exciting electric and magnetic fields. The nonlocal response approach has several merits. First, in the hard X-ray regime, the dipole (long wavelength) approximation may fail for certain material transitions. Deviation from the dipole approximation may also be observed at longer wavelengths when the current densities are highly delocalized. A nonlocal description that implicitly accounts for all higher multipoles is then called for. Expansion of the current into electric and magnetic multipole moments is possible but becomes tedious when higher multipoles are needed, while the nonlocal description leads to expressions that are only marginally more complicated than the dipole case. Second, the nonlocal response tensors are expressed in terms of physically intuitive elementary quantities: time dependent current and charge densities. Third, nonlocal response tensors encompass both the contribution of current **j** and charge σ densities, while the σ term is neglected in the dipole approximation. This allows us to describe pure σ interaction pathways, usually used in off-resonance diffraction applications or pure resonant **j** pathways that when integrated over space correspond to the standard resonant nonlinear optical pathways in the dipole approximation. Pathways that depend on both **j** and σ, and are relevant at intermediate detunings, can be accounted for. In near resonant diffraction, these mixed charge/current contributions are known as anomalous diffraction.[12]

The outline of this paper is as follow. First, we review the nonlocal response description of nonlinear spectroscopy. Formal expressions are derived for heterodyne detected (coherent, stimulated) signals as well as for spontaneous emission (incoherent) signals. In section 3, we use this formalism to simulate various heterodyne (stimulated) signals for thiophene at the sulfur K-edge. These include X-ray absorption (XAS) and stimulated X-ray Raman spectroscopy (SXRS). Spontaneous scattering signals are then discussed and formally linked to two-photon absorption in section 4.

2. NONLOCAL DESCRIPTION OF X-RAY SPECTROSCOPY

The nonlocal response formalism[13,14] starts with the minimal coupling field-matter interaction Hamiltonian:[15]

$$H_{\mathrm{int}}(t) = -\int d\mathbf{r}\mathbf{j}(\mathbf{r})\cdot\mathbf{A}(\mathbf{r}, t) - \frac{e}{2mc}\sigma(\mathbf{r})\mathbf{A}^2(\mathbf{r}, t) \tag{1}$$

where e and m are the electron charge and mass and $\mathbf{A}(\mathbf{r})$ is the vector potential.

$$\begin{aligned}\mathbf{j}(\mathbf{r}) &= \frac{e}{2m}(|r\rangle\langle r|p + p^\dagger|r\rangle\langle r|)\\ &= \frac{e\hbar}{2mi}(\psi^\dagger(\mathbf{r})\nabla\psi(\mathbf{r}) - (\nabla\psi(\mathbf{r})^\dagger)\psi(\mathbf{r}))\end{aligned} \tag{2}$$

is the current density operator, and

$$\sigma(\mathbf{r}) = e\psi^\dagger(\mathbf{r})\psi(\mathbf{r}) \tag{3}$$

is the charge density operator. Here, $\psi^\dagger(\mathbf{r})$ and $\psi(\mathbf{r})$ are the electron field Fermion creation and annihilation operators at position **r**. Also, p is the momentum operator. Note that the required molecular poperties, namely, the charge and the current densities are independent of the choice of origin.

We consider signals given by the rate of change of the photon occupation number N_s in the detected field mode s:

Received: March 17, 2016
Published: June 27, 2016

DOI: 10.1021/acs.jctc.6b00279
J. Chem. Theory Comput. 2016, 12, 3959−3968

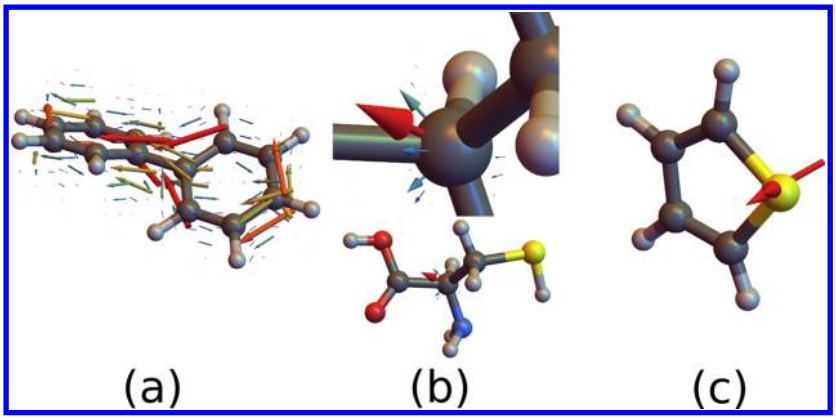

Figure 1. Current densities calculated using eq 10 for different typical wavelengths. (a) Valence excitation (5.96 eV) in biphenyl. (b) C K-edge excitation (282 eV) in cysteine (top figure is on an expanded scale). (c) S K-edge excitation (2.47 keV) in thiophene. The valence excitations for biphenyl have been calculated at the CIS/6-31G* level of theory, while the core excitations in cysteine and thiophene have been calculated using RASSCF (restricted active space self-consistent field) described in more detail in Section 3.

$$S(\mathbf{k}_s, \{\alpha_i\}) = \int dt \langle\langle \dot{N}_s | \rho_T(t) \rangle\rangle \tag{4}$$

Here, N_s is the number operator for photon in the mode s. Also, $|O\rangle\rangle$ denotes Liouville space vectors, and $\langle\langle A|B \rangle\rangle \triangleq \mathrm{Tr}(A^\dagger B)$ is the scalar product in Liouville space.[9] Here, $\rho_T(t)$ denotes the total (field and matter) density matrix, and $\rho(t)$ is the matter density matrix. The set α_i represents the parameters used in a specific signal (time delays, incoming wave vectors, etc.). These are specified in the following applications.

In Appendix A, we employ a quantum description of the detected field modes to obtain

$$S(\mathbf{k}_s, \{\alpha_i\}) = \frac{i}{\hbar} \int d\mathbf{r} dt \langle\langle \mathbf{J}(\mathbf{r}) \cdot \mathbf{A}(\mathbf{r}) | \rho_T(t) \rangle\rangle \tag{5}$$

The physical matter quantity that determines this signal is the gauge invariant electron current density[13]

$$\mathbf{J}(\mathbf{r}) = \mathbf{j}(\mathbf{r}) - \frac{e}{mc} \mathbf{A}(\mathbf{r}) \sigma(\mathbf{r}) \tag{6}$$

Assuming a classical optical field, we can recast eq 5 as

$$S(\mathbf{k}_s, \{\alpha_i\}) = \frac{i}{\hbar} \int dr \langle\langle \mathbf{J}(\mathbf{r}) | \rho(t) \rangle\rangle \cdot \mathbf{A}(\mathbf{r}, t) \tag{7}$$

$$\langle\langle \mathbf{J}(\mathbf{r}) | \rho(t) \rangle\rangle = \mathrm{Tr}[\mathbf{J}(\mathbf{r}) \exp_+(-i \int \mathcal{L}_{\mathrm{int}}(t)) \rho_{\mathrm{eq}}] \tag{8}$$

Here, $\exp_+$ is the time ordered exponential, ρ_{eq} is the stationary density matrix, and the interaction Liouvillian $\mathcal{L}_{\mathrm{int}}(r, t) = \tilde{H}_{\mathrm{int}}(r, t)$ is

$$\mathcal{L}_{\mathrm{int}}(t) = -\int d\mathbf{r} \tilde{\mathbf{j}}(\mathbf{r}) \cdot \mathbf{A}(\mathbf{r}, t) - \frac{e}{2mc} \tilde{\sigma}(\mathbf{r}) \mathbf{A}^2(\mathbf{r}, t) \tag{9}$$

The tilde denotes the commutation superoperator associated with a Hilbert space operator O, $\tilde{O}X \equiv [O,X]$. Equation 7 is known as the heterodyne detected signal, which represents the change of transmission of an incoming probe field.

Specific signals can be obtained by expanding the exponent in eq 8 pertubatively in $\mathcal{L}_{\mathrm{int}}(t)$. We refer to the nth-order term as $\mathcal{L}_{\mathrm{int}}^{(n)}$. We should then collect terms in powers of $\mathbf{A}$. Since $\mathcal{L}_{\mathrm{int}}(t)$ (eq 9) is both linear and quadratic in $\mathbf{A}$, $\mathcal{L}_{\mathrm{int}}^{(n)}$ will contain contributions to all orders between $\mathbf{A}^n$ to $\mathbf{A}^{2n}$. The common practice is to use the $\sigma\tilde{\mathbf{A}}^2$ coupling for off-resonant processes and the $\tilde{\mathbf{j}} \cdot \mathbf{A}$ coupling for resonant processes.[16] Hereafter, we examine the relative contributions of both terms, discuss the validity of the above approximations, and present some four-wave mixing signals that involve both resonant and off resonant contributions.

To first order in $\mathbf{A}$, the gauge invariant current density (eq 8) is

$$\mathbf{J}^{(1)}(\mathbf{r}, \omega) = -\frac{i}{\hbar} \int d\mathbf{r}_1 dt_1 \langle\langle \mathbf{j}(r) | \mathcal{G}(t_1) \tilde{j}(\mathbf{r}_1) \cdot \mathbf{A}(\mathbf{r}_1, \omega) e^{i\omega t_1} | \rho_{\mathrm{eq}} \rangle\rangle - \frac{e}{mc} \langle\langle \sigma(r) | \rho_{\mathrm{eq}} \rangle\rangle \mathbf{A}(\mathbf{r}, \omega) \tag{10}$$

where

$$\mathcal{G}(t) = \theta(t) \sum_{\nu\nu'} |\nu\nu'\rangle\rangle e^{-i\omega_{\nu\nu'} t - \Gamma_{\nu\nu'} t} \langle\langle \nu\nu' | \tag{11}$$

A sum-overstates expression for $\mathbf{J}^{(1)}(\mathbf{r},\omega)$ for an incoming Gaussian pulse is given in Appendix B. By displaying the total current density $\mathbf{J}(\mathbf{r},t)$ that generates the detected field, we can visualize the contribution of different regions in the molecule to the response. In Figure 1, the first-order current density $\mathbf{J}^{(1)}(\mathbf{r},\omega)$ given in eq 10 is displayed for various excitation wavelengths. The total current density is delocalized for optical transitions and becomes more localized for deeper core transitions. This is connected to the localization of the molecular orbitals of the states involved in the transition: The $\mathbf{j}$ term in eq 10 has a spatial extent comparable to the underlying core orbital, while the σ term, negligible at resonance, has a contribution that extends over the molecule.

Higher-order nonlinear current densities $\mathbf{J}^{(2)}$, $\mathbf{J}^{(3)}$, etc., which depend on various interaction delays between pulses, can provide a real space visualization of multidimensional signals.

2.1. Stimulated (Heterodyne-Detected) Third-Order Signals. Below, we give the expressions for time- and wave vector-resolved signals for impulsive pulses based on the results of references 13 and 14. Indices *i*, *ii*, and *iii* are used to denote the first-, second-, and third-order contribution in $\mathcal{L}_{\mathrm{int}}$, respectively. The third-order nonlocal response function is given by

$$S^{(3)}(\mathbf{k}_s, \mathbf{k}_1\mathbf{k}_2\mathbf{k}_3, t_1t_2t_3) = S^i + S^{ii} + S^{iii} \tag{12}$$

$$S^i = \left(\frac{-e}{mc}\right)\left(\frac{-e}{2mc}\right)\left(\frac{-i}{\hbar}\right) \langle\langle \sigma(\mathbf{k}_s - \mathbf{k}_3) I_{s,3} \delta(t_3) | \mathcal{G}(t_2) \tilde{\sigma}(\mathbf{k}_2 - \mathbf{k}_1) I_{2,1} \delta(t_1) | \rho_{\mathrm{eq}} \rangle\rangle \tag{13}$$

DOI: 10.1021/acs.jctc.6b00279
J. Chem. Theory Comput. 2016, 12, 3959−3968

$$S^{ii} = \left(\frac{-e}{2mc}\right)\left(\frac{-i}{\hbar}\right)^2 \langle\langle \mathbf{j}(\mathbf{k})|\mathcal{G}(t_3)\tilde{\sigma}(\mathbf{k}_3 - \mathbf{k}_2)I_{3,2}\delta(t_2)\mathcal{G}(t_1)\tilde{j}(\mathbf{k}_1)|\rho_{eq}\rangle\rangle + \left(\frac{-e}{2mc}\right)\left(\frac{-i}{\hbar}\right)^2 \langle\langle \mathbf{j}(\mathbf{k})|\mathcal{G}(t_3)\tilde{j}(\mathbf{k}_3)\mathcal{G}(t_2)\tilde{\sigma}(\mathbf{k}_2 - \mathbf{k}_1)I_{2,1}\delta(t_1)|\rho_{eq}\rangle\rangle + \left(\frac{-e}{mc}\right)\left(\frac{-i}{\hbar}\right)^2 \langle\langle \sigma(\mathbf{k}_s - \mathbf{k}_3)I_{s,3}\delta(t_3)|\mathcal{G}(t_2)\tilde{j}(\mathbf{k}_2)\mathcal{G}(t_1)\tilde{j}(\mathbf{k}_1)|\rho_{eq}\rangle\rangle \tag{14}$$

$$S^{iii} = \left(\frac{-i}{\hbar}\right)^3 \langle\langle \mathbf{j}(\mathbf{k})|\mathcal{G}(t_3)\tilde{j}(\mathbf{k}_3)\mathcal{G}(t_2)\tilde{j}(\mathbf{k}_2)\mathcal{G}(t_1)\tilde{j}(\mathbf{k}_1)\rho_{eq}\rangle\rangle \tag{15}$$

where $I_{i,j}$ denotes the identity matrix in the $i \otimes j$ direct product space and is used to indicate the scalar product with the vector potential of the associated space.

For classical optical fields, the heterodyne signal is given by

$$S_{het}(\mathbf{k}_s, \{\alpha_i\}) = \frac{i}{\hbar}\int d\mathbf{k}_s d\mathbf{k}_3 d\mathbf{k}_2 d\mathbf{k}_1 dt dt_3 dt_2 dt_1 S^{(3)}(\mathbf{k}_s, \mathbf{k}_1\mathbf{k}_2\mathbf{k}_3, t_1t_2t_3)\cdot(\mathbf{A}_s(\mathbf{k}_s, t) \otimes \mathbf{A}_3(\mathbf{k}_3, t - t_3) \otimes \mathbf{A}_2(\mathbf{k}_2, t - t_3 - t_2) \otimes \mathbf{A}_1(\mathbf{k}_1, t - t_3 - t_2 - t_1)) \tag{16}$$

where $\{\alpha_i\}$ stands for all pulse parameters. Assuming that the incoming pulses are temporally well separated, the interactions with the various pulses have a controlled time ordering. In this case, there are 22 possible interaction pathways (8 from S^{iii}, 12 from S^{ii}, and 2 from S^{i}) that can be represented by ladder diagrams. Adding the possibility to interact with either the positive or the negative frequency component of the vector potential for each interaction yields 22×16 ladder diagrams. The rules for calculating these diagrams in the dipole approximation are given in ref 9. Some additional rules are needed to extend them to the minimal coupling Hamiltonian and allow the possibility to interact either with σ or $\mathbf{j}$ (eq 1).

1. Each interaction with the current density brings a factor of $-i/\hbar$; each interaction with the charge density brings a factor of $-e/2mc$ ($-e/mc$ if this interaction is the last).
2. Each interaction with the charge density $\sigma(r_i)$ is accompanied by $\delta(r_{i+1}-r_i)\delta(t_1)$.

Depending on the level scheme and field frequencies, some diagrams may be neglected by invoking the rotating wave approximation (RWA), which simplifies the calculation. Moreover, the position of the detector will select only a subset of diagrams for a given phase matching direction. In the dipole approximation, the signal is generated along the directions $\pm\mathbf{k}_1 \pm \mathbf{k}_2 \pm \mathbf{k}_3$. In the nonlocal formalism, the pulses can come with a finite $\mathbf{k}$ space envelope (ultrafocused fields), and each diagram represents an emission in a cone. It is then necessary to sum over all the modes that the detector receives taking into account its position and spatial extent. For plane wave fields, one can eliminate the $\mathbf{k}$ space integrals in eq 16 but the signal will still depend on the incoming wave vector. This applies for example to diffraction.

2.2. Incoherent Scattering Signals. Fluorescence and diffraction are spontaneously emitted (scattering) signals. We assume that the detected field mode is initially in the vacuum state, and the field+matter density matrix prior to detection is $|\rho_T(t)\rangle\rangle = |\rho_M(t)\rangle\rangle \otimes |0_s\rangle\rangle$. If the matter is initially in its ground state, only the $\mathbf{J}(\mathbf{r})a_s$ contribution in eq 31 (Appendix A) survives the RWA. A zero-order expansion of the density matrix in eq 5 gives a vanishing signal. The density matrix must be expanded at least to first order in the interaction with the spontaneous mode s. The second interaction with the detected mode yields a nonvanishing field density matrix element and the trace over the field degrees of freedom no longer vanishes.

$$S_{sle}(\mathbf{k}_s) = \frac{i}{\hbar}\left(-\frac{i}{\hbar}\right)\int \langle\langle N_s|\left(\tilde{j}_s(r) - \frac{e}{2mc}\tilde{\sigma}_s(r)\cdot\mathbf{A}(r, t)\right) \times\mathcal{G}(t_1)\left(\tilde{j}_s(r_1) - \frac{e}{2mc}\tilde{\sigma}_s(r_1)\cdot\mathbf{A}(r_1, t - t_1)\right) \times|\rho_T(t - t_1) \otimes 0_s\rangle\rangle \tag{17}$$

where $\mathbf{j}_s(r) = \mathbf{j}(r)\cdot\mathbf{A}_s(r)$ and $\boldsymbol{\sigma}_s(r) = \boldsymbol{\sigma}(r)\cdot\mathbf{A}_s(r)$. Here, $\mathbf{A}$ with no subscript stands for externally applied field modes.

We have calculated all elements of this expansion using the matrix elements given in Appendix A. By tracing out the detected mode, the signal is finally recast in terms of purely matter correlation functions:

$$S_{sle}(\mathbf{k}_s) = \frac{\hbar}{2\epsilon_0 L^3\omega_s}\frac{2}{\hbar^2}\int d\mathbf{r}_s d\mathbf{r}'_s dt dt_s \langle\langle \mathbf{j}(\mathbf{r}_s)\cdot\mathbf{A}_s|\mathcal{G}(t_s)\tilde{j}(\mathbf{r}'_s)\cdot\mathbf{A}_s|\rho(t - t_s)\rangle\rangle + \left(-\frac{e}{mc}\right)\langle\langle \mathbf{j}(\mathbf{r}_s)\cdot\mathbf{A}_s|\mathcal{G}(t_s)\tilde{\sigma}(\mathbf{r}'_s)|\rho(t - t_s)\rangle\rangle\mathbf{A}_s\cdot\mathbf{A}(\mathbf{r}'_s, t - t_s) + \left(-\frac{e}{2mc}\right)\langle\langle \sigma(\mathbf{r}_s)|\mathcal{G}(t_s)\tilde{j}(\mathbf{r}'_s)\cdot\mathbf{A}_s|\rho(t - t_s)\rangle\rangle\mathbf{A}_s\cdot\mathbf{A}(\mathbf{r}_s, t) + \left(\frac{-e}{2mc}\right)\left(\frac{-e}{mc}\right)\langle\langle \sigma(\mathbf{r}_s)|\mathcal{G}(t_s)\tilde{\sigma}(\mathbf{r}'_s)|\rho(t - t_s)\rangle\rangle \mathbf{A}_s\cdot\mathbf{A}(\mathbf{r}_s, t)\mathbf{A}_s\cdot\mathbf{A}(\mathbf{r}'_s, t - t_s) \tag{18}$$

The density matrix may be expanded further in the incoming classical fields as it was done in the previous section. The signal is finally obtained by replacing the discrete sum over field modes by its mode density $\sum_i \to L^3\int d\omega_s\,(\omega_s^2/\pi^2c^3)$:

$$S_{sle}(\mathbf{k}_s) = \frac{\omega_s}{2\epsilon_0\pi^2c^3\hbar}\int d\mathbf{r}d\mathbf{r}'_s dt dt_s(S^1_{sle} + S^2_{sle} + S^3_{sle}) \tag{19}$$

$$S^1_{sle} = \langle\langle \mathbf{j}(\mathbf{r}_s)\cdot\boldsymbol{\epsilon}_s e^{i\mathbf{k}_s\cdot\mathbf{r}_s}|\mathcal{G}(t_s)\tilde{j}(\mathbf{r}'_s)\cdot\boldsymbol{\epsilon}_s|\rho(t - t_s)\rangle\rangle \tag{20}$$

$$S^2_{sle} = \left(-\frac{e}{2mc}\right)\langle\langle \mathbf{j}(\mathbf{r}_s)\cdot\boldsymbol{\epsilon}_s|\mathcal{G}(t_s)\tilde{\sigma}(\mathbf{r}'_s)|\rho(t - t_s)\rangle\rangle\boldsymbol{\epsilon}_s\cdot\mathbf{A}(\mathbf{r}'_s, t - t_s) + \left(-\frac{e}{2mc}\right)\langle\langle \sigma(\mathbf{r}_s)|\mathcal{G}(t_s)\tilde{j}(\mathbf{r}'_s)\cdot\boldsymbol{\epsilon}_s|\rho(t - t_s)\rangle\rangle\boldsymbol{\epsilon}_s\cdot\mathbf{A}(\mathbf{r}_s, t) \tag{21}$$

$$S^3_{sle} = \left(-\frac{e}{2mc}\right)^2\langle\langle \sigma(\mathbf{r}_s)|\mathcal{G}(t_s)\tilde{\sigma}(\mathbf{r}'_s)|\rho(t - t_s)\rangle\rangle \times \boldsymbol{\epsilon}_s\cdot\mathbf{A}(\mathbf{r}_s, t)\boldsymbol{\epsilon}_s\cdot\mathbf{A}(\mathbf{r}'_s, t - t_s) \tag{22}$$

Here, $\boldsymbol{\epsilon}_s$ is the polarization vector of the detected photon. In the absence of a polarized detection, one has to sum over polarizations.

Equations 19−22 may be used as a starting point for a pertubative expansion of the matter density matrix $|\rho(t-t_1)\rangle\rangle$ in the incoming fields thus yielding various types of multidimensional signals. The system may be excited by an arbitrary sequence of pulses and then evolves freely until the time $t-t_1$ where the measurement process starts as given by eq 22.

DOI: 10.1021/acs.jctc.6b00279
J. Chem. Theory Comput. 2016, 12, 3959−3968

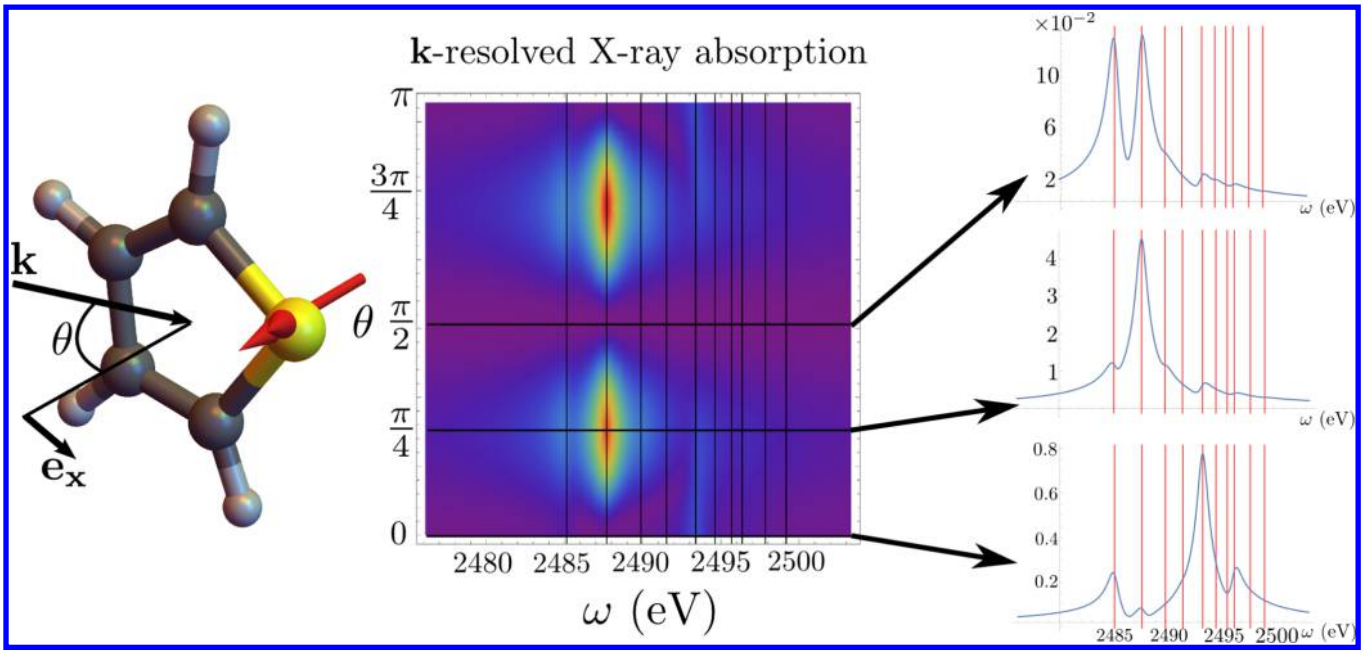

Figure 2. Wave vector-dependent X-ray absorption spectroscopy (XAS) signal (eq 23) at the sulfur K-edge of an oriented thiophene molecule versus the frequency and direction of the incoming linearly polarized Gaussian beam along the unit vector $\mathbf{e}_x$. On the right, XAS signals are displayed for some selected directions of the incoming pulse.

3. NONLINEAR SPECTROSCOPY AT THE SULFUR K-EDGE OF THIOPHENE

Core hole states in molecules can be calculated with, for example, the ΔSCF method, time-dependent density functional theory (TDDFT), and complete active space self-consistent field (CASSCF)-based method (for a broader overview see ref 5 and references therein). While TDDFT is very efficient for larger molecules, CASSCF-based methods can be readily applied to smaller molecules, providing a good balance between accuracy, flexibility, and calculation time. As a multiconfiguration method, it allows us to capture the involved valence states properly. Moreover a CASSCF calculation can be augmented with a multireference pertubative expansion to obtain highly accurate X-ray spectra.[17]

The low lying core states of the sulfur atom of thiophene make it a good marker for hard X-ray spectroscopy. The valence states are calculated with the package MOLPRO[18] at the CASSCF(6/5)/cc-pVTZ level of theory. To take into account the necessary relativistic corrections for the sulfur 1s electrons a second-order Douglas−Kroll−Hess Hamiltonian[19,20] is employed. The sulfur 1s core excited states are then obtained in a subsequent restricted active space calculation (RASSCF): The S(1s) orbital is rotated into the active space resulting in a RASSCF(8/6)/cc-pVTZ calculation, where the S(1s) orbital is restricted to single occupancy. The S(1s) molecular orbital coefficients are frozen in the wave function optimization to guarantee convergence to a core hole state rather than a valence state. The resulting lowest lying core hole transition is 2485 eV (compared to the experiment,[21] 2471 eV), which corresponds to an error <1%. All relevant quantities necessary to compute the nonlocal response are directly obtained from the MCSCF wave functions as described in Appendix C.

3.1. X-ray Absorption of Oriented Thiophene. We have simulated the transmission from an oriented thiophene at the sulfur K-edge (2.48 keV):

$$S_{\mathrm{XAS}}(\mathbf{k}_s, \omega) = \frac{i}{\hbar}\int d\mathbf{k} d\mathbf{k}_1 \langle\langle \mathbf{j}(\mathbf{k})\cdot\mathbf{A}_1(-\mathbf{k})|\mathcal{G}(\omega)\tilde{j}(\mathbf{k}_1)\cdot\mathbf{A}_1(-\mathbf{k}_1)|\rho_{\mathrm{eq}}\rangle\rangle - \frac{e}{mc}\int d\mathbf{k} d\mathbf{k}_1 \langle\langle \sigma(\mathbf{k}+\mathbf{k}_1)|\rho_{\mathrm{eq}}\rangle\rangle \mathbf{A}_s(-\mathbf{k})\cdot\mathbf{A}_1(-\mathbf{k}_1) \quad (23)$$

The $\mathbf{k}_s$ dependence comes from the vector potential of a plane wave with wave vector $\mathbf{k}_s$: $\mathbf{A}_1(\mathbf{k}) = \mathbf{A}_1\delta(\mathbf{k} - \mathbf{k}_s)$. From this expression, one can readily see that σ only contributes a frequency-independent background. However, its variation with $\mathbf{k}_s$ can still provide information about the molecular structure in the off-resonance regime where the current densities can be neglected.

Figure 2 depicts the signal (eq 23) versus the frequency and the direction of an incoming Gaussian beam. The beam central frequency is tuned at the sulfur K-edge, 2.48 keV, and is assumed to be ultrabroadband (tens of eV are achievable[22]). In the impulsive limit, the signal is given in eq 23. We used the sum-overstate expression given in Appendix D, eq 45. The transition at 2488 eV possesses a strong maximum when the incoming x polarized beam is incident with an angle of $\pi/4$. The symmetry of the angular dependence is due to the σ_v symmetry plane. The signal depends on the molecular orientation.

3.2. Stimulated X-ray Raman Signals. Stimulated X-ray Raman spectroscopy (SXRS)[23,24] is a technique that probes the electronic manifold through core excitation, making use of the ultrafast and broadband nature of X-ray pulses.

The technique uses a pump−probe configuration where each pulse interacts twice with the sample. It first creates a core excitation that can evolve for a short time before a second interaction with the same pulse destroys the core hole and generates a valence excitation. During the delay τ between the two pulses, the system is prepared in a superposition of valence states and the signal is recorded as a function of this delay. The beam geometry is displayed in Figure 3(a) (we assume two Gaussian pulses), and the level scheme is given is Figure 3(b). Both pulses are tuned at the sulfur K-edge (2.47 keV).

DOI: 10.1021/acs.jctc.6b00279
J. Chem. Theory Comput. 2016, 12, 3959−3968

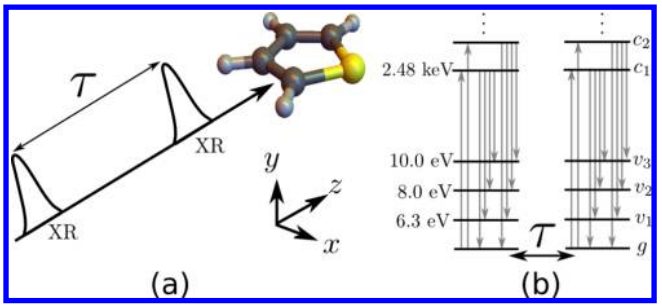

Figure 3. (a) Beam geometry used to measure the SXRS signal corresponding to the diagrams in Figure . (b) Energy levels of thiophene excited in SXRS.

All pulses are modeled as impulsive Gaussian beams propagating along the z axis and linearly polarized along y as given in Appendix E. Various beam configurations may be employed to monitor the spatial behavior of the current and charge densities. The diagrams describing the SXRS signal are given in Figure 4 Diagram (a) is a $\mathcal{L}_{\text{int}}^{(3)}$ process that is dominant near resonance. In the impulsive limit, the time integrals are eliminated, and the signal is simply proportional to the response function defined in eq 16. Using the diagrams in Figure 4, the SXRS signals is[23]

$$S_{\text{SXRS}}(\tau) = -\Re \int\int dt dt_1 dt_2 dt_3 d\mathbf{r} d\mathbf{r}_1 d\mathbf{r}_2 d\mathbf{r}_3 \times (S^{jjjj}_{\text{SXRS}}(\tau) + S^{\sigma jj}_{\text{SXRS}}(\tau) + S^{jj\sigma}_{\text{SXRS}}(\tau) + S^{\sigma\sigma}_{\text{SXRS}}(\tau)) \quad (24)$$

$$S_{\text{SXRS}}(\omega) = \frac{1}{(2\pi)^{1/2}} \int d\tau S_{\text{SXRS}}(\tau) e^{-i\omega\tau} \quad (25)$$

The final sum-overstates expressions used to calculate the signals are given in Appendix D, eqs 52−55. The time integrations appearing in eq 24 calculated for Gaussian pulses yield the final signal given in Appendix F, eq 60 The laser frequencies are tuned at the S K-edge and detuned by a value of $\Delta\omega$. The SXRS signals calculated for three values of $\Delta\omega$ (0, 15, and 40 eV) are displayed in Figure 5.

Figure 5 depicts contributions *i*, *ii*, and *iii* to the signal. The *ii* contribution contains two terms (eq 53 and 54) that are referred to as $jj\sigma$ and σjj. The $j\sigma j$ term does not contribute in SXRS because we assume that the two pulses do not overlap. By analogy, contribution *iii* may be referred as *jjjj* and the *i* one by $\sigma\sigma$. The relative contributions of the *jjjj*, $\sigma\sigma j$, $j\sigma\sigma$, and $\sigma\sigma$ terms as a function of the detuning are given in Figure 6. One can observe

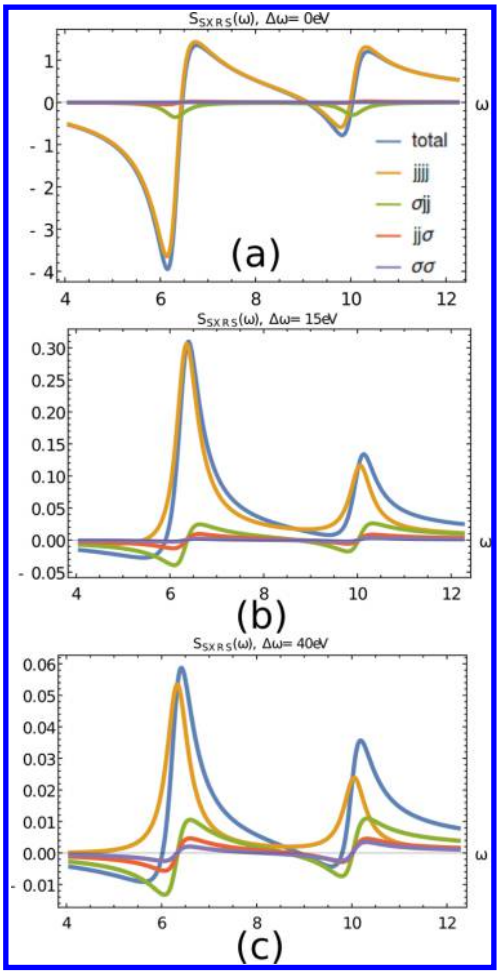

Figure 5. SXRS signals defined in eq 25 for different detuning value of the X-ray beam. One can observe that, when the exciting beams are not fully resonant, several terms must be considered to compute the total signals.

that the contributions of *i* and *ii* are small compared to *iii* when the pulses are resonant but dominate off-resonance. The relative strength of each contribution and its variation with frequency detuning is plotted for the valence excitation at 11 eV. Similar behavior is observed at other frequencies.

3.3. Time-Resolved Two-Photon Induced Fluorescence. Recently, Takamasu and co-workers[22] have reported two-photon absorption of a 5.6 keV XFEL beam in germanium detected by X-ray fluorescence and discussed the relative

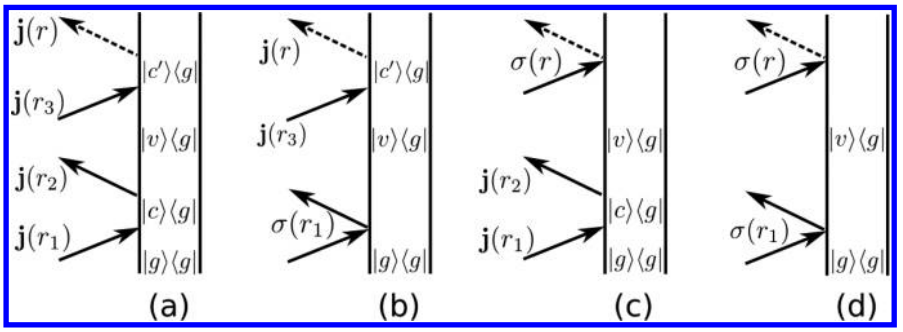

Figure 4. Diagrams used to calculate the SXRS signal defined in eq 24. In the nonlocal picture, one has to include interactions with the charge density (a), (b), and (c) on top of the contribution with only current density interaction (a). Diagram (a) corresponds to the standard SXRS signal in the local limit.[23] The full signal contains four more diagrams corresponding to the first two interactions acting on the bra on the density matrix.

DOI: 10.1021/acs.jctc.6b00279
J. Chem. Theory Comput. 2016, 12, 3959−3968

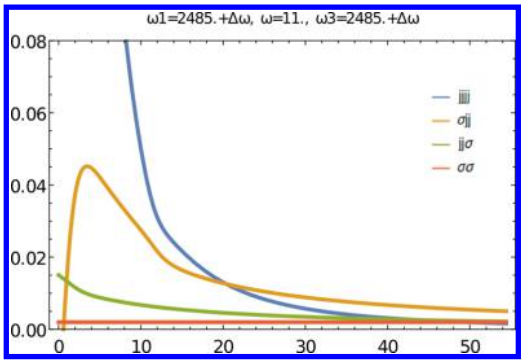

Figure 6. Different contributions to the SXRS signal (eq 24) as a function of the detuning. Near resonance, the *jjjj* process is strongly dominating the other ones. One can observe that other contributions than *jjjj* dominate off-resonance and that there exists an intermediate regime in which several terms must be considered.

contribution of the $\mathbf{j}\cdot\mathbf{A}$ and $\sigma\mathbf{A}^2$ terms. We now apply the nonlocal description to study these relative contributions. The analysis is very similar to the scattering discussed above: both are two-photon processes (up/down vs up/up).

Fluorescence[25] is a spontaneous incoherent signal, and we thus use eq 19 as a starting point. Diagrams representing different contributions to the signal are given in Figure 7(a) and (b), and a schematic of the pulses geometry is given in Figure 7(c).

Two photons (one visible, one X-ray) are first absorbed by the molecule, and the process is repeated after a delay τ. The *jjjj* contribution to the signal is represented in diagram (a):

$$S^{\mathrm{TPA}}_{jjjj}(\mathbf{k}_s,\tau)=\frac{1}{2\hbar\epsilon_0 c|\mathbf{k}_s|}\int d\mathbf{r}_s\dots d\mathbf{r}_1' dt\dots dt_1\langle\langle j^s(\mathbf{r}_s)e^{i\mathbf{k}_s\cdot\mathbf{r}_s}|\mathcal{G}(t_s)\tilde{j}^{s*}(\mathbf{r}_s')e^{i\mathbf{k}_s\cdot\mathbf{r}_s'}\mathcal{G}(\tau_s)\tilde{j}(\mathbf{r}_2)\mathcal{G}(t_2)\tilde{j}(\mathbf{r}_2')\mathcal{G}(\tau)\tilde{j}(\mathbf{r}_1)\mathcal{G}(t_1)\tilde{j}(\mathbf{r}_1')|\rho_{\mathrm{eq}}\rangle\rangle\cdot\mathbf{A}(\mathbf{r}_2,t-t_s-\tau_s)\mathbf{A}(\mathbf{r}_2',t-t_s-\tau_s-t_2)\times\mathbf{A}(\mathbf{r}_1,t-t_s-\tau_s-t_2-\tau)\times\mathbf{A}(\mathbf{r}_1',t-t_s-\tau_s-t_2-\tau-t_1) \quad (26)$$

In a similar way, the contributions of diagrams involving the charge density (Figure 7 (b)) are

$$S^{\mathrm{TPA}}_{\sigma\sigma}(\mathbf{k}_s,\tau)=\frac{1}{2\hbar\epsilon_0 c|\mathbf{k}_s|}\int d\mathbf{r}_s\dots d\mathbf{r}_1 dt\dots dt_1\langle\langle j^s(\mathbf{r}_s)e^{i\mathbf{k}_s\cdot\mathbf{r}_s}|\mathcal{G}(t_s)\tilde{j}^{s*}(\mathbf{r}_s')e^{i\mathbf{k}_s\cdot\mathbf{r}_s'}\mathcal{G}(\tau_s)\tilde{\sigma}(r_2)\mathcal{G}(\tau)\tilde{\sigma}(r_1)|\rho_{\mathrm{eq}}\rangle\rangle\times\mathbf{A}(\mathbf{r}_2,t-t_s-\tau_s)\cdot\mathbf{A}(\mathbf{r}_2,t-t_s-\tau_s)\times\mathbf{A}(\mathbf{r}_1,t-t_s-\tau_s-\tau)\cdot\mathbf{A}(\mathbf{r}_1,t-t_s-\tau_s-\tau) \quad (27)$$

$$S^{\mathrm{TPA}}_{jj\sigma}(\mathbf{k}_s,\tau)=\frac{1}{2\hbar\epsilon_0 c|\mathbf{k}_s|}\int d\mathbf{r}_s\dots d\mathbf{r}_1 dt\dots dt_1\langle\langle j^s(\mathbf{r}_s)e^{i\mathbf{k}_s\cdot\mathbf{r}_s}|\mathcal{G}(t_s)\tilde{j}^{s*}(\mathbf{r}_s')e^{i\mathbf{k}_s\cdot\mathbf{r}_s'}\mathcal{G}(\tau_s)\tilde{j}(r_2)\mathcal{G}(t_2)\tilde{j}(r_2')\mathcal{G}(\tau)\tilde{\sigma}(r_1)|\rho_{\mathrm{eq}}\rangle\rangle\times\mathbf{A}(\mathbf{r}_2,t-t_s-\tau_s)\cdot\mathbf{A}(\mathbf{r}_2',t-t_s-\tau_s)\times\mathbf{A}(\mathbf{r}_1,t-t_s-\tau_s-\tau)\cdot\mathbf{A}(\mathbf{r}_1,t-t_s-\tau_s-\tau) \quad (28)$$

However, the general spontaneous signals presented in eq 22 can be used to calculate other spontaneous signals. For example, homodyne detected signals for samples much larger than the wavelength of the incoming beams can be considered. Diffraction type measurements when one focuses on the **k** space distribution of the emission can also be calculated.

4. DISCUSSION

We have implemented a nonlocal response formulation of nonlinear X-ray signals based on the minimal coupling Hamiltonian for the light−matter interaction. The matter enters through the charge and current densities thus offering a real-space picture of the electron dynamics in the molecule. The focus has been put on X-ray spectroscopies because the dipole approximation is more likely to fail when the wavelength is comparable to the molecular size. In this article, we have demonstrated that the extension of the transition current densities scales with the incoming wavelength. However, the dipole approximation fails to consider nontrivial beam spatial variation and the charge densities contributions.

The nonlocal formalism, that avoids the multipolar expansion, may be used to describe both stimulated heterodyne-detected or spontaneous incoherent signals. In this paper, we have calculated X-ray absorption, stimulated X-ray Raman spectroscopy, and two-photon induced fluorescence signals. The standard resonant and off-resonant treatments that only retain the current densities or the charge density, respectively, are recovered. In anomalous X-ray scattering,[12] both quantities must be retained and are naturally included in the nonlocal formalism. Both current and charge densities then contribute substantially to the signals.

The nonlocal description of light−matter interaction offers many future possibilities. An obvious application would be the design of interactions of matter with a strongly spatially varying field. Such fields could be achieved experimentally at short wavelength, using the progresses of beam ultrafocusing or of nontrivial polarization state (such as radial or azimuthal polarization). The important progress in near-field optics can also lead to new exciting signals, using the near-field at the vicinity of a nanoparticle for example. We note that nonlocal effects already occur in spectroscopies that depend on the

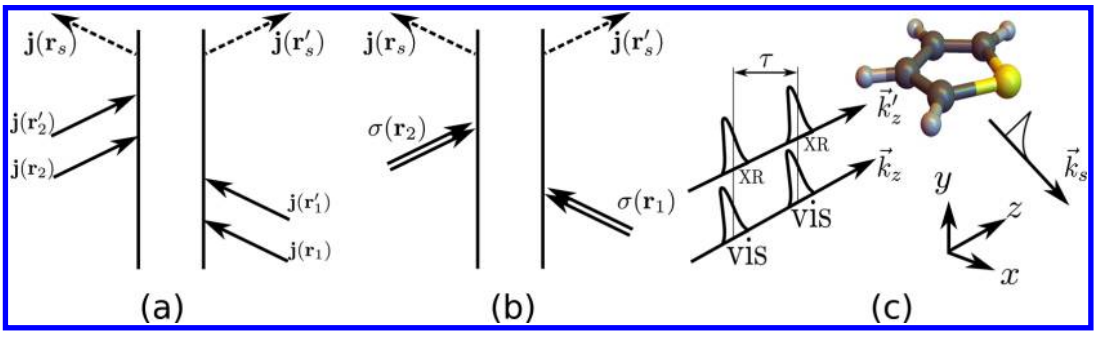

Figure 7. Ladder diagrams for two-photon fluorescence. As in Section 3.2, light−matter interaction is described by current densities (a) and charge densities (b). (c) Beam geometry used to model the measurement of time-resolved two-photon absorption fluorescence.

DOI: 10.1021/acs.jctc.6b00279
J. Chem. Theory Comput. 2016, 12, 3959−3968

magnetic dipole, for example, circular dichroism. Additionally, joint current and charge density interactions that can occur in nonlinear optical experiments can be accounted for in the nonlocal description.

APPENDIX A: DERIVATION OF EQ 5

Using the Liouville−Von Neumann equation, the rate of change of the occupation number is readily expressed as $\dot{N}_s = i/\hbar \mathcal{L}_{\text{int}}(r) a_s^\dagger a_s$. Here, $\mathcal{L}_{\text{int}}(r)$ is defined in eq 9 with classical vector potential that are now replaced by their quantum operators:

$$\mathbf{A}(\mathbf{r}) = \sum_i \mathbf{A}_i a_i + \mathbf{A}_i^* a_i^\dagger \tag{29}$$

$$\mathbf{A}_i(\mathbf{r}) = \sqrt{\frac{\hbar}{2\epsilon_0 \omega_i L^3}}\, \boldsymbol{\epsilon}_i e^{i\mathbf{k}_i\cdot\mathbf{r}} \tag{30}$$

We detect the field s mode, and $\boldsymbol{\epsilon}_i$ is the polarization of this mode. We then define $\mathbf{j}^+ = j a_s^\dagger$, $\mathbf{j}^- = j a_s$, $\sigma^{2+} = \sigma a_s^\dagger a_s^\dagger$, $\sigma^0 = \sigma$, $\sigma^{2-} = \sigma a_s a_s$, and the corresponding Liouville space operators. Using these definitions, the photon rate of change becomes

$$\dot{N}_s = -\frac{i}{\hbar}\int d\mathbf{r} \tilde{j}^+(r)\cdot\mathbf{A}_s^*(\mathbf{r}) a_s^\dagger a_s + \tilde{j}^-(r)\cdot\mathbf{A}_s(\mathbf{r}) a_s^\dagger a_s - \frac{e}{2mc}(\tilde{\sigma}^0(\mathbf{r})\mathbf{A}_s\cdot\mathbf{A}_s^* + \tilde{\sigma}^{2-}(\mathbf{r})\mathbf{A}_s\cdot\mathbf{A}_s + \tilde{\sigma}^{2+}(\mathbf{r})\mathbf{A}_s^*\cdot\mathbf{A}_s^*) a_s^\dagger a_s \tag{31}$$

These operator products can be simplified using

$$\tilde{j}^+(r)\cdot\mathbf{A}_s^*(\mathbf{r}) a_s^\dagger a_s = -\mathbf{j}^+\cdot\mathbf{A}_s^*(\mathbf{r}) \tag{32}$$

$$\tilde{\sigma}^{2+}(\mathbf{r}) a_s^\dagger a_s = -2\sigma^{2+} \tag{33}$$

and the following matrix elements:

$$\langle\langle a_s | \tilde{a}_s | 0_s \rangle\rangle = -1 \tag{34}$$

$$\langle\langle a_s^\dagger | \tilde{a}_s^\dagger | 0_s \rangle\rangle = 1 \tag{35}$$

$$\langle\langle a_s a_s | \tilde{\sigma}^{2-} | 0_s \rangle\rangle = -2\sigma \tag{36}$$

$$\langle\langle a_s^\dagger a_s^\dagger | \tilde{\sigma}^{2+} | 0_s \rangle\rangle = 2\sigma \tag{37}$$

Inserting these expressions in eq 4 leads to the signal given in eq 5.

APPENDIX B: EXPRESSIONS FOR $J(R,T)$ AND $J(R,\omega)$

In this appendix, we provide a sum-overstate expression for $J(r,\omega)$ defined in eq 10. At the linear order, the time-dependent current density given in eq 8 is

$$\mathbf{J}^{(1)}(\mathbf{r}, t) = -\frac{i}{\hbar}\int d\mathbf{r}_1 dt_1 \langle\langle \mathbf{j}(r) | \mathcal{G}(t_1) \tilde{j}(\mathbf{r}_1)\cdot\mathbf{A}(\mathbf{r}_1, t - t_1) | \rho_{\text{eq}} \rangle\rangle - \frac{e}{mc}\langle\langle \sigma(r) | \rho_{\text{eq}} \rangle\rangle \mathbf{A}(\mathbf{r}, t) \tag{38}$$

If we assume an ultrashort pulse (Dirac δ function in time), the integral over t_1 is simplified and the current density becomes

$$\mathbf{J}^{(1)}(\mathbf{r}, t) = \frac{1}{\hbar}\sum_m \mathbf{j}_{gm}(r)\left(\frac{\int d\mathbf{r}_1 \mathbf{j}_{mg}(\mathbf{r}_1)\cdot\mathbf{A}(\mathbf{r}_1, \omega)}{\omega - \omega_{mg} + i\Gamma_{mg}} + \frac{\int d\mathbf{r}_1 \mathbf{j}_{mg}^*(\mathbf{r}_1)\cdot\mathbf{A}(\mathbf{r}_1, \omega)}{\omega + \omega_{mg} + i\Gamma_{mg}}\right) - \frac{e}{mc}\sigma_{gg}(\mathbf{r})\mathbf{A}(\mathbf{r}, \omega) \tag{39}$$

This is the formula used to compute the current densities displayed in Figure 1. Alternatively, we can consider a temporal Gaussian profile for the incoming pulse $\mathbf{A}(\mathbf{r}_1, t-t_1) = \mathbf{A}(\mathbf{r}_1) e^{-(t-t_1)^2/2\sigma^2} e^{-i\omega_L t_1} + c.c.$ The current density is given by

$$\mathbf{J}^{(1)}(\mathbf{r}, t) = -\frac{i}{\hbar}\sigma\sqrt{2\pi}\sum_m \mathbf{j}_{gm}(\mathbf{r})\int d\mathbf{r}_1 \mathbf{j}_{mg}(\mathbf{r}_1)\cdot\mathbf{A}(\mathbf{r}_1) \times \text{Re}\left(e^{i(\omega_L-\omega_{mg})t - \Gamma_{mg}t} e^{1/2\sigma^2(\Gamma_{mg} - i(\omega_L-\omega_{mg}))^2}\left(1 + \text{erf}\left(\frac{t}{\sqrt{2}\sigma} - \frac{\sigma}{2}(\Gamma_{mg} - i(\omega_L - \omega_{mg}))\right)\right)\right) \tag{40}$$

APPENDIX C: ELECTRON CURRENTS FROM MCSCF WAVE FUNCTIONS

In this section, we briefly review how the electron currents from eq 2 necessary for the spectra calculation can be obtained from a configuration interaction (CI) type wave function. The electron current $\mathbf{j}(\mathbf{r})$ can be expressed in terms of the full real valued electronic eigenstates $\Psi_i \equiv \Psi_i(\mathbf{r},\mathbf{r}_2,...,\mathbf{r}_N)$:

$$\mathbf{j}(\mathbf{r}) = \frac{1}{2}\sum_{i,j\neq i}^{M} \rho_{ij}\mathbf{j}_{ij}(\mathbf{r}) = \frac{1}{2}\sum_{i,j\neq i}\rho_{ij}\int d\mathbf{r}_2 ... d\mathbf{r}_N(\Psi_i\nabla\Psi_j - \Psi_j\nabla\Psi_i) \tag{41}$$

where the sum runs over all electronic states involved. Note that the diagonal elements ($i = j$) do not contribute as the current for any real valued, nondegenerate eigenstate vanishes. Here, ρ_{ij} is the density of matrix element of the electronic states. The wave function is then further expanded in a multiconfiguration self-consistent field (MCSCF) wave function

$$\Psi_i = \sum_m A_{mi}\Phi_m \tag{42}$$

such that the transition current reads

$$\mathbf{j}_{ij}(\mathbf{r}) = \int d\mathbf{r}_2 ... d\mathbf{r}_N \sum_{m,n\neq m} A_{mi}A_{nj}(\Phi_m\nabla\Phi_n - \Phi_n\nabla\Phi_m)$$

where A_{mi} is the CI coefficients of state i, configuration m, and Φ_m its corresponding Slater determinant. The transition currents are one-electron properties, meaning Brillouins theorem[26] applies and only combinations of determinants Φ_m and Φ_n differing in exactly one orbital need to be considered. The contributing determinants can be defined through

$$|\Phi_n\rangle = a_\mu^\dagger a_\nu |\Phi_m\rangle \tag{43}$$

where $a_\mu^\dagger$and a_ν create and annihilate an electron in spin orbital μ and ν, respectively. The current for MCSCF wave functions is then determined by the molecular orbital pairs $\psi_\mu^{(m)}(\mathbf{r})$ and $\psi_\nu^{(n)}(\mathbf{r})$ generated from configurations m and n:

DOI: 10.1021/acs.jctc.6b00279
J. Chem. Theory Comput. 2016, 12, 3959−3968

$$\mathbf{j}(\mathbf{r}) = \frac{1}{2}\sum_{i,j\neq i}\rho_{ij}\sum_{m,n\neq m}A_{mi}A_{nj}(\psi_\mu^{(m)}\nabla\psi_\nu^{(n)} - \psi_\nu^{(n)}\nabla\psi_\mu^{(m)}) \tag{44}$$

The time dependence of $\mathbf{j}$ enters through the coherences ρ_{ij}, whereas the time-independent quantities (A and ψ) have been obtained from the MCSCF calculation.

APPENDIX D: SUM-OVERSTATES EXPRESSIONS FOR X-RAY SIGNALS

In this section, we provide explicit expression for the different signals considered in this paper. The linear X-ray absorption signal is defined in eq 23. We assume an x polarized plane wave excitation $\mathbf{A}_1(\mathbf{k}) = \mathbf{e}_x A_1\delta(\mathbf{k}-\mathbf{k}_s)$. We vary the incident angle on the incoming pulse according to Figure 2. In the RWA approximation, the signal is given by

$$S_{\mathrm{XAS}}(\theta,\omega) = -\frac{i}{\hbar}\sum_m \frac{\mathbf{j}_{gm}(R_x(\theta)|\mathbf{k}_s|\mathbf{e}_y)\cdot\mathbf{A}_1\mathbf{j}^*_{mg}(R_x(\theta)|\mathbf{k}_s|\mathbf{e}_y)\cdot\mathbf{A}_1}{\omega-\omega_{mg}+i\Gamma_{mg}} - \frac{e}{mc}\sigma_{gg}(R_x(\theta)|\mathbf{k}_s|\mathbf{e}_y)\mathbf{A}_1\cdot\mathbf{A}_1 \tag{45}$$

where $R_x(\theta)$ is the rotation matrix around the x axis by an angle θ.

We give sum-overstate expression for the complete third-order response function.

$$S^{(3)}(\mathbf{r},\mathbf{r}_1\mathbf{r}_2\mathbf{r}_3,t_1,t_2,t_3) = S^{iii}_{jjjj} + S^{ii}_{jj\sigma} + S^{ii}_{j\sigma j} + S^{ii}_{\sigma jj} + S^{i}_{\sigma\sigma} \tag{46}$$

$$S^{i}_{\sigma\sigma} = \left(\frac{-e}{2mc}\right)\left(\frac{-e}{mc}\right)\left(+\sigma_{gm}(\mathbf{r})\mathcal{G}_{mg,\mathrm{mg}}(t_2)\sigma_{mg}(\mathbf{r}_2) - \sigma_{mg}(\mathbf{r})\mathcal{G}_{gm,\mathrm{gm}}(t_2)\sigma^*_{mg}(\mathbf{r}_2)\right) \tag{47}$$

$$\begin{aligned}S^{ii}_{jj\sigma} = \left(\frac{-i}{\hbar}\right)^2\left(\frac{-e}{2mc}\right)\Big(&+j_{gm}(\mathbf{r})\mathcal{G}_{mg,\mathrm{mg}}(t_3)j_{ma}(\mathbf{r}_3)\mathcal{G}_{ag,\mathrm{ag}}(t_2)\sigma_{ag}(\mathbf{r}_1)\\ &- j_{ma}(\mathbf{r})\mathcal{G}_{am,\mathrm{am}}(t_3)j^*_{mg}(\mathbf{r}_3)\mathcal{G}_{ag,\mathrm{ag}}(t_2)\sigma_{ag}(\mathbf{r}_1)\\ &- j_{am}(\mathbf{r})\mathcal{G}_{ma,\mathrm{ma}}(t_3)j_{mg}(\mathbf{r}_3)\mathcal{G}_{ga,\mathrm{ga}}(t_2)\sigma^*_{ag}(\mathbf{r}_1)\\ &- j_{mg}(\mathbf{r})\mathcal{G}_{gm,\mathrm{gm}}(t_3)j^*_{ma}(\mathbf{r}_3)\mathcal{G}_{ga,\mathrm{ga}}(t_2)\sigma^*_{ag}(\mathbf{r}_1)\Big)\end{aligned} \tag{48}$$

$$\begin{aligned}S^{ii}_{j\sigma j} = \left(\frac{-i}{\hbar}\right)^2\left(\frac{-e}{2mc}\right)\Big(&+j_{gm}(\mathbf{r})\mathcal{G}_{mg,\mathrm{mg}}(t_3)\sigma_{ma}(\mathbf{r}_3)\mathcal{G}_{ag,\mathrm{ag}}(t_1)j_{ag}(\mathbf{r}_1)\\ &- j_{ma}(\mathbf{r})\mathcal{G}_{am,\mathrm{am}}(t_3)\sigma^*_{mg}(\mathbf{r}_3)\mathcal{G}_{ag,\mathrm{ag}}(t_1)j_{ag}(\mathbf{r}_1)\\ &- j_{am}(\mathbf{r})\mathcal{G}_{ma,\mathrm{ma}}(t_3)\sigma_{mg}(\mathbf{r}_3)\mathcal{G}_{ga,\mathrm{ga}}(t_1)j^*_{ag}(\mathbf{r}_1)\\ &- j_{mg}(\mathbf{r})\mathcal{G}_{gm,\mathrm{gm}}(t_3)\sigma^*_{ma}(\mathbf{r}_3)\mathcal{G}_{ga,\mathrm{ga}}(t_1)j^*_{ag}(\mathbf{r}_1)\Big)\end{aligned} \tag{49}$$

$$\begin{aligned}S^{iii}_{jjjj} = \left(\frac{-i}{\hbar}\right)^3\Big(&+j_{gm}(\mathbf{r})\mathcal{G}_{gm,\mathrm{gm}}(t_3)j_{ma}(\mathbf{r}_3)\mathcal{G}_{ag,\mathrm{ag}}(t_2)j_{ac}(\mathbf{r}_2)\mathcal{G}_{cg,\mathrm{cg}}(t_1)j_{cg}(\mathbf{r}_1)\\ &- j_{cm}(\mathbf{r})\mathcal{G}_{cm,\mathrm{cm}}(t_3)j_{ma}(\mathbf{r}_3)\mathcal{G}_{ac,\mathrm{ac}}(t_2)j_{ag}(\mathbf{r}_2)\mathcal{G}_{gc,\mathrm{gc}}(t_1)j^*_{cg}(\mathbf{r}_1)\\ &- j_{am}(\mathbf{r})\mathcal{G}_{am,\mathrm{am}}(t_3)j_{mc}(\mathbf{r}_3)\mathcal{G}_{ca,\mathrm{ca}}(t_2)j^*_{ag}(\mathbf{r}_2)\mathcal{G}_{cg,\mathrm{cg}}(t_1)j_{cg}(\mathbf{r}_1)\\ &- j_{ma}(\mathbf{r})\mathcal{G}_{ma,\mathrm{ma}}(t_3)j^*_{mg}(\mathbf{r}_3)\mathcal{G}_{ag,\mathrm{ag}}(t_2)j_{ac}(\mathbf{r}_2)\mathcal{G}_{cg,\mathrm{cg}}(t_1)j_{cg}(\mathbf{r}_1)\\ &+ j_{am}(\mathbf{r})\mathcal{G}_{am,\mathrm{am}}(t_3)j_{mg}(\mathbf{r}_3)\mathcal{G}_{ga,\mathrm{ga}}(t_2)j^*_{ac}(\mathbf{r}_2)\mathcal{G}_{gc,\mathrm{gc}}(t_1)j^*_{cg}(\mathbf{r}_1)\\ &+ j_{ma}(\mathbf{r})\mathcal{G}_{ma,\mathrm{ma}}(t_3)j^*_{mc}(\mathbf{r}_3)\mathcal{G}_{ac,\mathrm{ac}}(t_2)j_{ag}(\mathbf{r}_2)\mathcal{G}_{gc,\mathrm{gc}}(t_1)j^*_{cg}(\mathbf{r}_1)\\ &+ j_{mc}(\mathbf{r})\mathcal{G}_{mc,\mathrm{mc}}(t_3)j^*_{ma}(\mathbf{r}_3)\mathcal{G}_{ca,\mathrm{ca}}(t_2)j^*_{ag}(\mathbf{r}_2)\mathcal{G}_{cg,\mathrm{cg}}(t_1)j_{cg}(\mathbf{r}_1)\\ &- j_{mg}(\mathbf{r})\mathcal{G}_{mg,\mathrm{mg}}(t_3)j^*_{mc}(\mathbf{r}_3)\mathcal{G}_{ga,\mathrm{ga}}(t_2)j^*_{ac}(\mathbf{r}_2)\mathcal{G}_{gc,\mathrm{gc}}(t_1)j^*_{cg}(\mathbf{r}_1)\Big)\end{aligned} \tag{51}$$

In Section 3.2, the SXRS signal is calculated using the following expressions, derived from the diagrams in Figure 4.

$$\begin{aligned}S^{jjjj}_{\mathrm{SXRS}} = &\sum_{cc'v}\mathbf{j}_{gc'}(\mathbf{r})\cdot\mathbf{A}^*_2(\mathbf{r},t-\tau)\mathbf{j}_{c'v}(\mathbf{r}_3)\cdot\mathbf{A}_2(\mathbf{r}_3,t_3-\tau)\\ &\mathrm{e}^{-i\omega_L(t_3-t)}\Big(\mathbf{j}_{vc}(\mathbf{r}_2)\cdot\mathbf{A}^*_1(\mathbf{r}_2,t_2)\mathbf{j}_{cg}(\mathbf{r}_1)\cdot\mathbf{A}_1(\mathbf{r}_1,t_1)\\ &\mathrm{e}^{-i\omega_{c'g}t+i\omega_{c'v}t_3-i\omega_{cv}t_2+i\omega_{cg}t_1-i\omega_L(t_1-t_2)}+\mathbf{j}_{vc}(\mathbf{r}_2)\cdot\mathbf{A}_1(\mathbf{r}_2,t_2)\\ &\mathbf{j}_{cg}(\mathbf{r}_1)\cdot\mathbf{A}^*_1(\mathbf{r}_1,t_1)\mathrm{e}^{-i\omega_{cv}t+i\omega_{cg}t_3+i\omega_{c'v}t_2-i\omega_{c'g}t_1+i\omega_L(t_1-t_2)}\Big)\end{aligned} \tag{52}$$

$$\begin{aligned}S^{jj\sigma}_{\mathrm{SXRS}} = &\sum_{cv}\left(-\frac{e}{mc}\sigma_{gv}(r)\delta(r-r_3)\delta(t-t_3)\right)\\ &\times\mathbf{A}^*_2(\mathbf{r},t-\tau)\cdot\mathbf{A}_2(\mathbf{r}_3,t_3-\tau)\\ &\times\Big(\mathbf{j}_{vc}(\mathbf{r}_2)\cdot\mathbf{A}^*_1(\mathbf{r}_2,t_2)\mathbf{j}_{cg}(\mathbf{r}_1)\cdot\mathbf{A}_1(\mathbf{r}_1,t_1)\\ &\mathrm{e}^{-i\omega_{c'g}t+i\omega_{c'v}t_3-i\omega_{cv}t_2+i\omega_{cg}t_1-i\omega_L(t_1-t_2)}\\ &+\mathbf{j}_{vc}(\mathbf{r}_2)\cdot\mathbf{A}_1(\mathbf{r}_2,t_2)\mathbf{j}_{cg}(\mathbf{r}_1)\cdot\mathbf{A}^*_1(\mathbf{r}_1,t_1)\\ &\mathrm{e}^{-i\omega_{cv}t+i\omega_{cg}t_3+i\omega_{c'v}t_2-i\omega_{c'g}t_1+i\omega_L(t_1-t_2)}\Big)\end{aligned} \tag{53}$$

$$\begin{aligned}S^{\sigma jj}_{\mathrm{SXRS}} = &\sum_{c'v}\mathbf{j}_{gc'}(\mathbf{r})\cdot\mathbf{A}^*_2(\mathbf{r},t-\tau)\mathbf{j}_{c'v}(\mathbf{r}_3)\cdot\mathbf{A}_2(\mathbf{r}_3,t_3-\tau)\mathrm{e}^{-i\omega_L(t_3-t)}\\ &\Big(\left(-\frac{e}{2mc}\sigma_{vg}(r)\delta(r_2-r_1)\delta(t_2-t_1)\right)\\ &\times\mathbf{A}^*_1(\mathbf{r}_2,t_2)\cdot\mathbf{A}_1(\mathbf{r}_1,t_1)\mathrm{e}^{-i\omega_{c'g}t+i\omega_{c'v}t_3-i\omega_{cv}t_2+i\omega_{cg}t_1}\\ &+\left(-\frac{e}{2mc}\sigma_{vg}(r)\delta(r_2-r_1)\delta(t_2-t_1)\right)\\ &\times\mathbf{A}_1(\mathbf{r}_2,t_2)\cdot\mathbf{A}^*_1(\mathbf{r}_1,t_1)\mathrm{e}^{-i\omega_{cv}t+i\omega_{cg}t_3+i\omega_{c'v}t_2-i\omega_{c'g}t_1}\Big)\end{aligned} \tag{54}$$

DOI: 10.1021/acs.jctc.6b00279
J. Chem. Theory Comput. 2016, 12, 3959−3968

$$
\begin{aligned}
S^{\sigma\sigma}_{\mathrm{SXRS}} = \sum_{v} & \left(-\frac{e}{mc}\sigma_{gv}(r)\delta(r-r_3)\delta(t-t_3)\right) \\
& \times \mathbf{A}_2^*(\mathbf{r}, t-\tau)\cdot\mathbf{A}_2(\mathbf{r}_3, t_3-\tau) \\
& \left(\left(-\frac{e}{2mc}\sigma_{vg}(r)\delta(r_2-r_1)\delta(t_2-t_1)\right)\right. \\
& \times \mathbf{A}_1^*(\mathbf{r}_2, t_2)\cdot\mathbf{A}_1(\mathbf{r}_1, t_1)\mathrm{e}^{-i\omega_{c'g}t+i\omega_{c'v}t_3-i\omega_{cv}t_2+i\omega_{cg}t_1}+ \\
& \left(-\frac{e}{2mc}\sigma_{vg}(r)\delta(r_2-r_1)\delta(t_2-t_1)\right) \\
& \left.\times \mathbf{A}_1(\mathbf{r}_2, t_2)\cdot\mathbf{A}_1^*(\mathbf{r}_1, t_1)\mathrm{e}^{-i\omega_{cv}t+i\omega_{cg}t_3+i\omega_{c'v}t_2-i\omega_{c'g}t_1}\right)
\end{aligned} \tag{55}
$$

APPENDIX E: IMPULSIVE GAUSSIAN BEAMS

The monochromatic linearly polarized Gaussian beam propagating along the z axis in the paraxial approximation is given by

$$
\mathbf{A}(r, z, \omega) = \mathbf{A}_0\frac{w_0}{w(z)}e^{-r^2/w^2(z)}\mathrm{e}^{-i(kz-\omega t)-ikr^2/2R(z)+i\zeta(z)} + c.c. \tag{56}
$$

where $w(z)$ is the beam waist, $R(z)$ is the radius of curvature, and $\zeta(z)$ is the Gouy phase.[27] We further assumed an infinite Rayleigh length. Thus, the beam divergence along the z axis is neglected. This is justified by the small extension of a molecule compared to a typical Rayleigh length (few microns). The Gaussian beam has a much simpler expression:

$$
\mathbf{A}(r, z, \omega) = \mathbf{A}_0 e^{-r^2/w_0^2}\mathrm{e}^{-i(kz-\omega t))} + c.c. \tag{57}
$$

A Gaussian time envelope for the Gaussian beam is obtained by choosing a Gaussian frequency distribution and carrying out the Fourier transform of the previous equation:

$$
\mathbf{A}(r, z, t) = \frac{\mathbf{A}_0}{\sqrt{2\pi}}e^{-r^2/w_0^2}e^{-4\ln 2/\Delta t^2(t-\tau-\frac{z}{c})^2}\mathrm{e}^{-i(kz-\omega t))} + c.c. \tag{58}
$$

where Δt is the fwhm and τ is the retardation of the pulse. In the impulsive limit, the beam takes the form used throughout this article to calculate integrated components of the current and charge densities:

$$
\mathbf{A}(r, z, t) = \sqrt{2\pi}\mathbf{A}_0 e^{-r^2/w_0^2}\delta\left(t-\tau-\frac{z}{c}\right) \tag{59}
$$

APPENDIX F: FINAL EXPRESSIONS FOR SXRS

In this appendix, we give the SXRS signal (eq 24) using eqs 52−55 in Appendix D and the definition of the vector potential given in Appendix E, eq 58 for a pulse with a finite duration.

$$
\begin{aligned}
S_{\mathrm{SXRS}}(\tau) = & -\pi\sigma_1^2\sigma_2^2\Re\sum_{cvc'}\boldsymbol{\mu}^2_{gc'}\cdot\mathbf{A}_2^*\boldsymbol{\mu}^2_{c'v}\cdot\mathbf{A}_2\boldsymbol{\mu}^1_{vc}\cdot\mathbf{A}_1^*\boldsymbol{\mu}^1_{cg}\cdot\mathbf{A}_1\mathrm{e}^{-i\omega_{vg}\tau-\Gamma_{vg}\tau} \\
& e^{-\sigma_2^2(\omega_{vg}+i(\Gamma_{c'v}+\Gamma_{c'g}))^2+(2\omega_2-\omega_{c'v}-\omega_{c'g}+i(\Gamma_{c'v}+\Gamma_{c'g}))^2/4} \\
& \times\mathrm{erfc}\left(-i\sigma_2\frac{2\omega_2-\omega_{c'v}-\omega_{c'g}+i(\Gamma_{c'v}+\Gamma_{c'g})}{2}\right) \\
& e^{-\sigma_1^2(\omega_{gv}+i(\Gamma_{cg}+\Gamma_{cv}))^2+(2\omega_1-\omega_{cg}-\omega_{cv}+i(\Gamma_{cg}+\Gamma_{cv}))^2/4} \\
& \times\mathrm{erfc}\left(-i\sigma_1\frac{2\omega_1-\omega_{cg}-\omega_{cv}+i(\Gamma_{cg}+\Gamma_{cv})}{2}\right) \\
& +\boldsymbol{\mu}^2_{vc'}\cdot\mathbf{A}_2^*\boldsymbol{\mu}^2_{c'g}\cdot\mathbf{A}_2\boldsymbol{\mu}^1_{vc}\cdot\mathbf{A}_1\boldsymbol{\mu}^1_{cg}\cdot\mathbf{A}_1^*\mathrm{e}^{-i\omega_{gv}\tau-\Gamma_{gv}\tau} \\
& e^{-\sigma_2^2(\omega_{gv}+i(\Gamma_{c'g}+\Gamma_{c'v}))^2+(2\omega_2-\omega_{c'g}-\omega_{c'v}+i(\Gamma_{c'g}+\Gamma_{c'v}))^2/4} \\
& \times\mathrm{erfc}\left(-i\sigma_2\frac{2\omega_2-\omega_{c'g}-\omega_{c'v}+i(\Gamma_{c'g}+\Gamma_{c'v})}{2}\right) \\
& e^{-\sigma_1^2(\omega_{gv}+i(\Gamma_{cg}+\Gamma_{cv}))^2+(2\omega_1-\omega_{cg}-\omega_{cv}+i(\Gamma_{cg}+\Gamma_{cv}))^2/4} \\
& \times\mathrm{erfc}\left(+i\sigma_1\frac{2\omega_1-\omega_{cg}-\omega_{cv}+i(\Gamma_{cg}+\Gamma_{cv})}{2}\right)
\end{aligned} \tag{60}
$$

where σ_i is related to the fwhm of the ith pulse by $\Delta t_i = 2\sqrt{\ln 2}\,\sigma_i$. The spatially integrated current densities $\boldsymbol{\mu}^i_{mn}$ are given by $\boldsymbol{\mu}^i_{mn} = \int d\mathbf{r}A_i(\mathbf{r})\mathbf{j}_{mn}(\mathbf{r})$, where $A_i(\mathbf{r})$ is the spatial profile of the incoming beam. For example, for a Gaussian beam incoming from the z axis, discussed in Appendix E, $A_i(\mathbf{r}) = 1/\sqrt{2\pi}\,e^{-r^2/w_i^2}e^{-\mathrm{i}k_i z}$.

AUTHOR INFORMATION

Corresponding Authors

*E-mail: jrouxel@uci.edu (J.R.R.).
*E-mail: mkowalew@uci.edu (M.K.).
*E-mail: smukamel@uci.edu (S.M.).

Notes

The authors declare no competing financial interest.

ACKNOWLEDGMENTS

The support of the Chemical Sciences, Geosciences, and Biosciences Division, Office of Basic Energy Sciences, Office of Science, U.S. Department of Energy through Award No. DE-FG02-04ER15571 and of the National Science Foundation (Grant No. CHE-1361516) is gratefully acknowledged. J.R was supported by the DOE grant. M.K. gratefully acknowledges support from the Alexander von Humboldt Foundation through the Feodor Lynen program.

REFERENCES

(1) Ding, Y.; Huang, Z.; Ratner, D.; Bucksbaum, P.; Merdji, H. Generation of attosecond X-ray pulses with a multicycle two-color enhanced self-amplified spontaneous emission scheme. *Phys. Rev. Spec. Top.–Accel. Beams* **2009**, *12*, 060703.

(2) Novotny, L.; van Hulst, N. Antennas for light. *Nat. Photonics* **2011**, *5*, 83.

(3) Zhang, Y.; Biggs, J. D.; Hua, W.; Dorfman, K. E.; Mukamel, S. Three-dimensional attosecond resonant stimulated X-ray Raman spectroscopy of electronic excitations in core-ionized glycine. *Phys. Chem. Chem. Phys.* **2014**, *16*, 24323−24331.

(4) Minitti, M. P.; Budarz, J. M.; Kirrander, A.; Robinson, J. S.; Ratner, D.; Lane, T. J.; Zhu, D.; Glownia, J. M.; Kozina, M.; Lemke, H. T.; et al. Imaging Molecular Motion: Femtosecond X-Ray Scattering of an Electrocyclic Chemical Reaction. *Phys. Rev. Lett.* **2015**, *114*, 255501.

(5) Zhang, Y.; Hua, W.; Bennett, K.; Mukamel, S. Nonlinear Spectroscopy of Core and Valence Excitations Using Short X-Ray

DOI: 10.1021/acs.jctc.6b00279
J. Chem. Theory Comput. 2016, 12, 3959−3968

Pulses: Simulation Challenges. In *Density-Functional Methods for Excited States*; Ferré, N., Filatov, M., Huix-Rotllant, M., Eds.; Springer International Publishing: Cham, 2016; pp 273−345.
(6) Moerner, W. E. Nobel Lecture: Single-molecule spectroscopy, imaging, and photocontrol: Foundations for super-resolution microscopy*. *Rev. Mod. Phys.* **2015**, *87*, 1183−1212.
(7) Berweger, S.; Atkin, J. M.; Xu, X. G.; Olmon, R. L.; Raschke, M. B. Femtosecond Nanofocusing with Full Optical Waveform Control. *Nano Lett.* **2011**, *11*, 4309−4313. , PMID: 21879749.
(8) Kao, T. S.; Rogers, E. T. F.; Ou, J. Y.; Zheludev, N. I. Digitally Addressable Focusing of Light into a Subwavelength Hot Spot. *Nano Lett.* **2012**, *12*, 2728−2731.
(9) Mukamel, S. *Principles of Non-Linear Optical Spectroscopy*; Oxford, 1995.
(10) Olsen, J.; Jorgensen, P. Linear and nonlinear response functions for an exact state and for an MCSCF state. *J. Chem. Phys.* **1985**, *82*, 3235.
(11) Helgaker, T.; Coriani, S.; Jørgensen, P.; Kristensen, K.; Olsen, J.; Ruud, K. Recent Advances in Wave Function-Based Methods of Molecular-Property Calculations. *Chem. Rev.* **2012**, *112*, 543−631.
(12) Son, S.-K.; Chapman, H. N.; Santra, R. Determination of multiwavelength anomalous diffraction coefficients at high x-ray intensity. *J. Phys. B: At., Mol. Opt. Phys.* **2013**, *46*, 164015.
(13) Chernyak, V. Y.; Saurabh, P.; Mukamel, S. Non-linear non-local molecular electrodynamics with nano-optical fields. *J. Chem. Phys.* **2015**, *143*, 164107.
(14) Tanaka, S.; Chernyak, V.; Mukamel, S. Time-resolved x-ray spectroscopies: Nonlinear response functions and Liouville-space pathways. *Phys. Rev. A: At., Mol., Opt. Phys.* **2001**, *63*, 063405.
(15) Salam, A. In *Molecular Quantum Electrodynamics: Long-Range Intermolecular Interactions*; Wiley, 2010.
(16) Cohen-Tannoudji, C.; Dupont-Roc, J.; Grynberg, G. In *Photons and Atoms: Introduction to Quantum Electrodynamics*; Wiley, 1989.
(17) Josefsson, I.; Kunnus, K.; Schreck, S.; Föhlisch, A.; de Groot, F.; Wernet, P.; Odelius, M. Ab Initio Calculations of X-ray Spectra: Atomic Multiplet and Molecular Orbital Effects in a Multiconfigurational SCF Approach to the L-Edge Spectra of Transition Metal Complexes. *J. Phys. Chem. Lett.* **2012**, *3*, 3565−3570.
(18) Werner, H.-J.; Knowles, P. J.; Knizia, G.; Manby, F. R.; Schütz, M. MOLPRO, version 2015.1, a package of ab initio programs, 2015. http://www.molpro.net (accessed July 2016).
(19) Douglas, M.; Kroll, N. M. Quantum electrodynamical corrections to the fine structure of helium. *Ann. Phys.* **1974**, *82*, 155.
(20) Hess, B. A. Relativistic electronic-structure calculations employing a two-component no-pair formalism with external-field projection operators. *Phys. Rev. A: At., Mol., Opt. Phys.* **1986**, *33*, 3742.
(21) George, G. N.; Hackett, M. J.; Sansone, M.; Gorbaty, M. L.; Kelemen, S. R.; Prince, R. C.; Harris, H. H.; Pickering, I. J. Long-Range Chemical Sensitivity in the Sulfur K-Edge X-ray Absorption Spectra of Substituted Thiophenes. *J. Phys. Chem. A* **2014**, *118*, 7796−7802.
(22) Tamasaku, K.; Shigemasa, E.; Inubushi, Y.; Katayama, T.; Sawada, K.; Yumoto, H.; Ohashi, H.; Mimura, H.; Yabashi, M.; Yamauchi, K.; et al. X-ray two-photon absorption competing against single and sequential multiphoton processes. *Nat. Photonics* **2014**, *8*, 313.
(23) Biggs, J. D.; Zhang, Y.; Healion, D.; Mukamel, S. Two-dimensional stimulated resonance Raman spectroscopy of molecules with broadband X-ray pulses. *J. Chem. Phys.* **2012**, *136*, 174117.
(24) Zhang, Y.; Biggs, J. D.; Mukamel, S. Understanding excitation energy transfer in metalloporphyrin heterodimers with different linkers, bonding structures, and geometries through stimulated X-ray Raman spectroscopy. *J. Mod. Opt.* **2014**, *61*, 558−567.
(25) Millar, D. P. Time-resolved fluorescence spectroscopy. *Curr. Opin. Struct. Biol.* **1996**, *6*, 637−642.
(26) Szabo, A.; Ostlund, N. S. *Modern Quantum Chemistry*; Dover Publications: New York, 1996.
(27) Pampaloni, F.; Enderlein, J. Gaussian, Hermite-Gaussian, and Laguerre-Gaussian beams: A primer. ArXiv Physics e-prints 2004.

DOI: 10.1021/acs.jctc.6b00279
J. Chem. Theory Comput. 2016, 12, 3959−3968